Advances in Basic and Applied Sciences 2 (2024) 20-28

Advances in Basic and Applied Sciences

journal homepage: https://abas.journals.ekb.eg/

# Impact of Samarium Ions in the Structural and Optical Characteristics of Aluminum-Sodium Phosphate Glasses

D. A. Rayan[1,2], A. M. Abdelghany[3], A. Elshourbgy[4], M. Hammam[5], S. H. Moustafa[5*]

[1]*Central Metallurgical Research & Development Institute, P.O. Box: 87 Helwan 11421, Cairo, Egypt*
[2]*Deraya University, Minia, Egypt*
[3]*Spectroscopy Department, Physics Research Institute, National Research Centre, 33 El-Behouth St., Dokki, 12622, Cairo, Egypt*
[4]*Giza Higher Institute for Engineering & Technology, Giza, Egypt*
[5]*Physics Department, Faculty of Science, Helwan University, Cairo, Egypt*

**ARTICLE INFO**

**Article history:**
Received 15 April 2023
Received in revised form 18 August 2023
Accepted 28 November 2023
Available online 31 January 2024

doi: 10.21608/ABAS.2023.206120.1020

**Keywords:** Samarium ions; Phosphate glass; XRD; Optical Absorption; FTIR.

## ABSTRACT

The glass structure $50P_2O_5–30Na_2O–10CaO–(10-x)Al_2O_3–(x)Sm_2O_3$ was prepared using a standard melt annealing method, where x ranged from 0 to 8 mol% and with different $Sm_2O_3$ (x) concentrations. The impact of $Sm^{3+}$ ions in the produced glass network has been investigated using combined structural and optical properties. We looked at structural and optical factors like density, molar volume, and other optical properties. It was demonstrated that glassy samples are amorphous using X-ray diffraction. Empirical and experimental densities and molar volume are found to be having the same trend with increasing $Sm_2O_3$ contents. Fourier transform infrared absorption spectra (FTIR) have been carried out and analyzed using the deconvolution analysis route. Notable changes are observed within the fingerprint region from 450 $cm^{-1}$ to 1700 $cm^{-1}$ and prominent peaks are assigned to their respective phosphate vibrational groups. UV–VIS–NIR spectral data are plotted and different optical parameters such as optical energy gap, absorption and extension coefficients are calculated and interpreted in terms of direct and indirect transitions and correlated to their respective structural variations and state of samarium ions.

.

## 1. Introduction

During the last decades' glasses with different formers (silicate, borate, phosphate, and their combinations) doped with variable mass fractions of rare earth ions are extensively used in broadband optical amplifiers [1–3], optical

* **Corresponding author E-mail:** s.moustafa@science.helwan.edu.eg

temperature sensors, near-infrared solid-state lasers [4], up-conversion systems [5–7] and optical coherence tomography [8]. According to *4f-4f* intra-configuration transitions rare earth oxides are considered to be optical active materials and play a vital role in the technology of lighting displays. Oxyfluoride phosphate glasses that are doped with a specific percent of specified rare earth oxides can be considered superior host materials in the process of laser production [9–18]. Glasses are painstaking as a good host for the higher content of rare earth ions owes an amorphous nature compared to other glassy matrices. The optical and structural characteristics of newly designed materials may be well defined using different spectroscopic routs including Infrared and Ramman spectroscopy depending on the type of host matrix and practical applications at which it may be used including the source of glass host emitting visible light [19–25] or (NIR) near-infrared radiation [26–28]. Contrasting with lead-free phosphate host glassy matrix, researchers devise less documentation of NIR and Vis. luminescence studies of rare earth-doped lead phosphate glasses. Based on spectroscopic and thermal characterization techniques, it can be concluded that glasses containing rare earth oxides owe a fascinating thermo-optical characteristic [29-31] in addition to the non-linear optical properties [29–31]. In cerium-doped lead phosphate glass, significant advancements in the second harmonic generation (SHG) are also seen [33]. In general, the addition of PbO to phosphate glasses raises the host's refractive indices, which is advantageous when producing holey fibres. These glasses are appropriate for optical device applications and a potential contender for radiation protection systems in the future, as evidenced by the observed shift in the absorption edge to higher energies with increased PbO content [34]. Various physical and spectroscopic characteristics of the different $Sm^{3+}$ doped sodium aluminum phosphate glasses in the nominal composition ($P_2O_5$–$Na_2O$–CaO–$Al_2O_3$) including density, molar volume in addition to optical electronic transition in the UV/Vis/NIR region (transmission (*T*), absorption (*A*), and refractive index (*n*)) combined with structure information supplied by XRD have been claimed in this work to inspect the effect of samarium oxide and aluminum oxide molar ratio on sodium phosphate glass for visible devices as optical fiber amplifiers applications.

## 2. Materials and Methods

### *2.1 Preparation of the glasses*

Transparent glasses of nominal composition 50 $P_2O_5$ – 30 $Na_2O$ –10 CaO – (10-*x*) $Al_2O_3$ – (*x*) $Sm_2O_3$ where *x* from 0 to 8 *mol%* are prepared via ordinary melt route. $P_2O_5$ was obtained using ammonium dehydrogenates phosphate ($NH_4H_2PO_4$), and Samarium oxide supplied by Sigma Aldrich company was added to the basic composition at expense of both main components of the base host glass. The weighed batches are mixed thoroughly and ground for 20-30 *min* in a ball mailing machine calcined for about 1 *h* in a 500 *°C* regulated electric furnace (Vecstar) to evaporate all ammonia and water residuals. The temperature was then gradually increased to 1300 °C to complete the melting and mixing process (which took 2 hours) to produce samples devoid of bubbles. To obtain a uniform, bubble-free viscous melt, viscous melts are switched at regular intervals. The obtained melt was then put into moulds made of stainless steel that met the specifications. To relieve the samples' thermal stresses, the produced glass samples are immediately placed in an annealing muffle furnace set at 300 °C.

### *2.2 Sample characterizations*

X-ray diffraction (XRD) is a strong non-destructive method in which crystalline materials are characterized. It offers data about constructions, stages, and preferred orientations of crystals (texture). X-ray diffraction peaks are created at particular corners from each set of lattice planes in a sample by constructive interference of the X-ray beam. The maximum intensities are determined by the lattice atom distribution. Because of this, an XRD-Shimadzu diffractometer's pattern of X-ray diffraction can be used to identify regular atomic structures in a given material. The glass system was examined using an advanced X-ray powder diffractometer (Brucker D8) and crystallographic data software (Topas 2) at room temperature. Cu target and Ni filter are used to produce a monochromatic Cu- $K_\alpha$ X-ray beam with a wavelength of 1.452 radiation running at 40 kV and 30 mA at a pace of 2°/min by placing a thin flat sheet in the path of the X-ray beam. The diffraction data was collected for $2\theta$ values ranging from 4° to 70°. Using the conventional Archimedes method, density is measured, and the results are used to value a number of structural factors. Many inorganic compounds' chemical structures are ascertained using Fourier Transform Infrared (FTIR) Spectroscopy, which is also utilised for qualitative and quantitative analyses of organic molecules. Using a Fourier transform computerised infrared spectrometer type (JASCO, FT-IR-6800, Japan), the FTIR absorption spectra of the glass samples are shown in terms of the wavenumber (range: 4000-400 $cm^{-1}$ with resolution 0.07 $cm^{-1}$) at atmospheric temperature. A two beam spectrophotometer (JASCO model V750 Japan) encompassing the range 200-2500 nm at room temperature was used to record the optical absorption spectral data for a highly polished sample both before and after adding dopant samarium oxide to the glasses. The various 1155 measurement points are used with a sample interval of 2 nm and a resolution limit of 0.2 nm.

## 3. Results and Discussion

### *3.1. Structural analysis*

Fig. 1 presents the XRD diffraction pattern of powdered samples from $Sm^{3+}$ ion doped sodium phosphate glass $50P_2O_5$- $30Na_2O$ – 10CaO – (10-*x*) $Al_2O_3$ – (*x*) $Sm_2O_3$ (*x* = 0, 2, 4, 6 and 8 *mol%)*. Obtained data confirm the amorphous nature of all prepared samples without any evidence for crystallization supported by the absence of any sharp peaks within the measurement region.

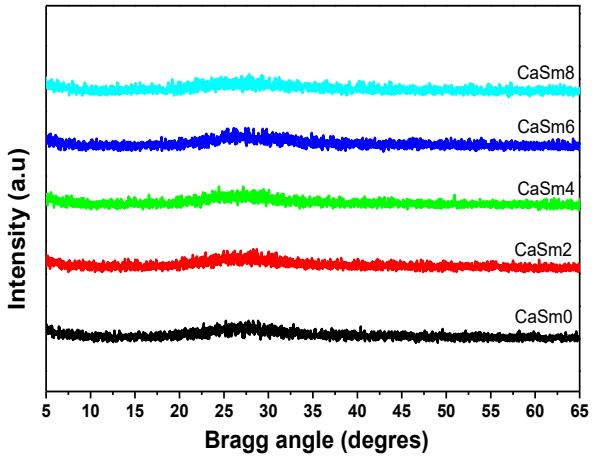


**Fig. 1:** X-ray diffraction patterns of $Sm^{3+}$ ion doped aluminum sodium phosphate glass (*x* = 0, 2, 4, 6 and 8 *mol%*).

### *3.2 Density and the Molar volume*

Density in relation to molar volume of $Sm^{3+}$ ion doped aluminum sodium phosphate glass [50 $P_2O_5$- 30 $Na_2O$ – 10 CaO – (10-*x*) $Al_2O_3$ – (*x*) $Sm_2O_3$] (*x* = 0, 2, 4, 6 and 8 *mol%*) was measured. The results are introduced in **Fig. 2** and **Table 1**. Both physical quantities (density $\rho$, molar volume $V_M$) are calculated according to relations:

$$\rho = [\frac{w_{air}}{w_{air}-w_l}]\rho_0 \quad (1)$$

$$V_M = [\frac{M_{w(glass)}}{\rho_{glass}}] \quad (2)$$

where $\rho$ is the sample density, $\rho_o$ the liquid density, $W_{air}$ is the weight in the air, $W_l$ is the weight in the liquid, $V_M$ is the molar volume, and $M_w$ is the molar mass. The density of the glass samples rises as $Sm^{3+}$ ion doped increases, as well as the molar volume and density, which increases proportionally to the $Sm^{3+}$ ion doped content as shown in **Fig. 2** and listed in **Table 1**.

The molar mass of samarium oxide (348.72 *g/mol*) is heavier than the molar mass of Aluminum oxide (101.96 *g/mol*) [35-37]. The glass matrix with larger samarium oxide content $Sm^{+3}$ is therefore denser. Moreover, due to the atomic radius of $Sm^{+3}$ ions (242 *pm*), the rise in molar volume is greater than the atomic radius of $Al^{+3}$ ions (118 *pm*) [38]. Unusual results, however, changed the molar volume and density with the same trend in the direction of each other, the usual being the molar volume and the opposite density changed. $Sm_2O_3$ has elevated relative molecular mass that opens the glass network framework and introduces a surplus quantity of structure. $Al_2O_3$ acts as a modifier and replacing $Al_2O_3$ with $Sm_2O_3$ causes the total molar volume to increase [39].

**Table 1:** Density and molar volume of $Sm^{3+}$ ion doped aluminum sodium phosphate glass

| *Sm mol %* | *Exp Density ($g/cm^3$)* | *Empirical Density ($g/cm^3$)* | *Exp MV($cm^3$/mol)* | *Empirical MV ($cm^3$/mol)* |
|---|---|---|---|---|
| **0** | 2.59 | 2.60 | 67.79 | 67.69 |
| **2** | 2.62 | 2.69 | 69.05 | 67.31 |
| **4** | 2.67 | 2.78 | 69.56 | 66.95 |
| **6** | 2.71 | 2.86 | 70.50 | 66.60 |
| **8** | 2.75 | 2.95 | 71.79 | 66.30 |

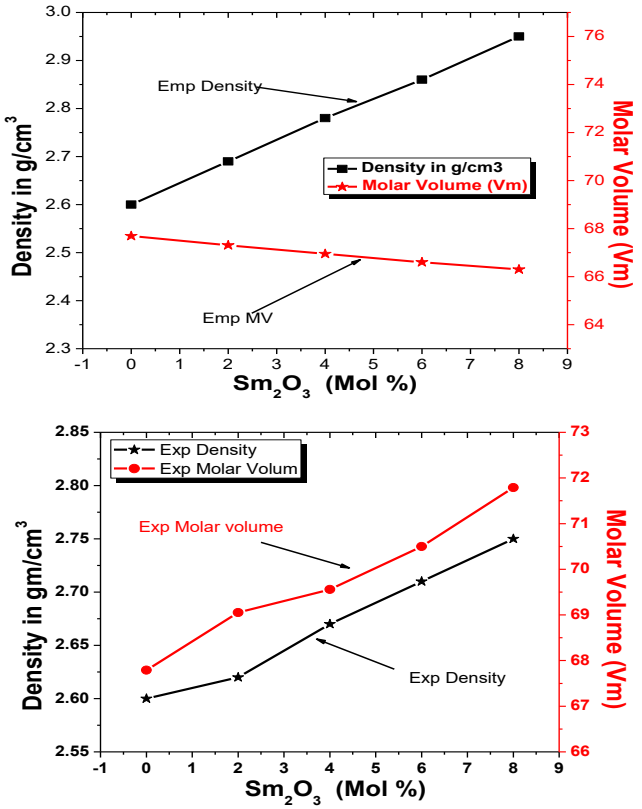


**Fig. 2:** Variation of a) the empirical density and the empirical molar volume and b) the experimental density and the experimental molar volume of aluminum sodium phosphate glass with different $Sm_2O_3$ contents.

### *3.3 Fourier Transform Infrared (FTIR) Spectroscopy*

One method to evaluate the chemical composition of

such samples is the FT-IR technique where the absorption, transmission, or reflection IR spectra show some peaks in terms of the wavenumber that corresponds to the existence of a kind of atomic bond for a specific molecule. FT-IR absorbance spectrum of $Sm^{3+}$ ion doped aluminum sodium phosphate glass matrix is recorded in **Fig. 6**. The aluminum phosphate glass FT-IR range was diverse with the aluminum coordinating number and the coordinating group state ("isolated" or condensed") in addition to the coupling among neighboring groups. Absorption bands in the region between 530-400 $cm^{-1}$ may be assigned to the isolated $AlO_6$octahedra while that lie between 680–500 $cm^{-1}$ are related to the condensed $AlO_6$ octahedra [40].

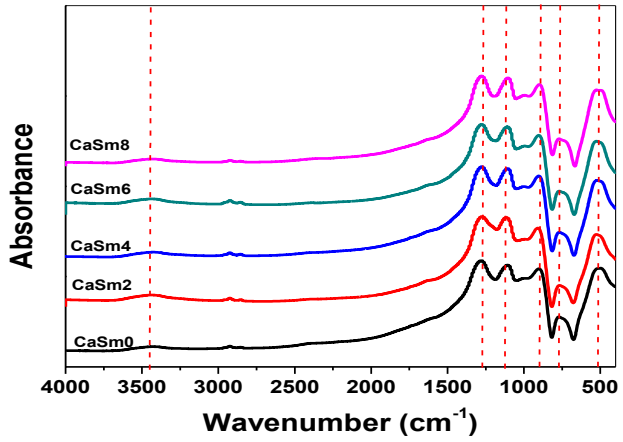


**Fig. 3:** FTIR of $Sm^{3+}$ ion doped aluminum sodium phosphate glass ($x$ = 0, 2, 4, 6 and 8 *mol%*)

Additionally, the condensed $AlO_4$ tetrahedra found in the region of 900-700 $cm^{-1}$ are indexed whereas the isolated $AlO_4$ tetrahedra found in the range of 800-650 $cm^{-1}$ are identified [40]. At 978 and 1170 $cm^{-1}$, a pair of peak bands connected to the Al-OH bonding are found [42]. The "isolated" and "condensed" $AlO_4$ tetrahedra and "isolated" and "condensed" $AlO_6$ octahedra's characteristic absorption zones of Al-O stretching vibrations are indexed. Due to the stretching vibration of Sm(III)-O groups, the absorption bands in Fig. 3 are linked to a very small number of $Sm^{+3}$ ions at 860 $cm^{-1}$ [43]. Otherwise, the bands' peak at 685.6 $cm^{-1}$ correlated with the Sm-O-H vibration and the broadband at 698 $cm^{-1}$ attributable to Sm-O-Sm vibrations are both present [44]. But a little IR peak at 3400 $cm^{-1}$ was found and linked to the O-H stretching vibration [45]. Additionally, showed vibrational bands at 1287 $cm^{-1}$ (detonate-symmetrical $PO^{2-}$ groups vibrations; this region may also contain bands from P=O stretching vibrations), 1082 $cm^{-1}$ (a regular vibrational mode in $PO_4^{3-}$ group arising from $n^3$-symmetric stretching), and 897 $cm^{-1}$ (due to P-O-P asymmetric bending vibrations). There may be bands in this area that are caused by pyrophosphate groups ($P_2O_7^4$). There are P-O-H wagging and rocking vibrational bands at 590 and 530 $cm^{-1}$ [46].

### *3.4 Optical properties*

The physical properties of the glasses, the calculated values of density ($\rho$) and refractive index along with other physical parameters such as absorbance coefficient, optical band gap energy, permittivity ($\varepsilon'$ and $\varepsilon''$), extinction coefficient, the refractive index was calculated using conventional formulae.

#### *3.4.1 Absorbance Coefficient*

The optical absorption spectrum of $Sm^{3+}$ ion doped aluminum sodium phosphate glass matrix deduced in the UV-Visible-NIR spectrum (200-2400 *nm*) region was shown in **Fig. 4**. This spectrum consists of inhomogeneous bands of diverse intensities due to *f-f* transitions of $Sm^{3+}$ ions to various excited states. The optical absorption spectrum displays thirteen transitions bands at wavelengths 249, 401, 470, 942, 1075, 1223, 1372, 1471, 1529, and 1593 *nm* which corresponds to excited states $^6H_{9/2}$, $^4D_{3/2}$, $^4L_{17/2}$, $^5P_{3/2}$, $^5P_{5/2}$, $^4L_{11/2}$, $^6F_{11/2}$, $^6F_{9/2}$, $^6F_{7/2}$, $^6F_{5/2}$, $^6F_{3/2}$, $^6F_{1/2}$ and $^6H_{13/2}$, respectively. Higher energy transitions in the UV-Visible range (300 - 500 nm) and lower energy transitions in the NIR area (1000 - 2400 nm) are the two groups into which these transitions are categorized [47, 49]. Higher energy transitions and lower energy transitions are separated into two groups, respectively. These transitions' UV-visible area intensity is lower than their NIR region intensity. This is explained by the host glass's enhanced UV-visible absorption and the overlaying of different 2S+1LJ levels. The transitions from the 6H5/2 energy level to the *6F*, *6H*, and 6P are all allowed for spin ($\Delta S = 0$), however the transitions from the *6H5/2* to *4I*, *4M*, *4L*, and *4D* are disallowed for spin ($\Delta J = 0, \pm 1$). However, the NIR transition $^6H_{5/2} \rightarrow {}^6F_{7/2}$ (1223 nm) is a hypersensitive transition because of its great intensity. The strength of this transition can be influenced by the surrounding environment of the ligand that follows the selection rules $\Delta S=0$, $\Delta L \leq 2$, and $\Delta J \leq 2$ [50–52].

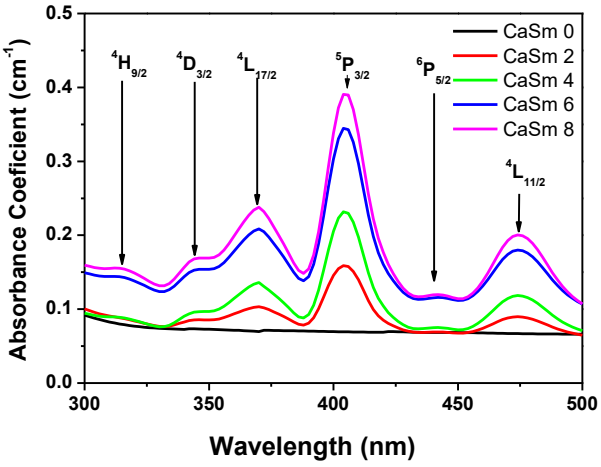

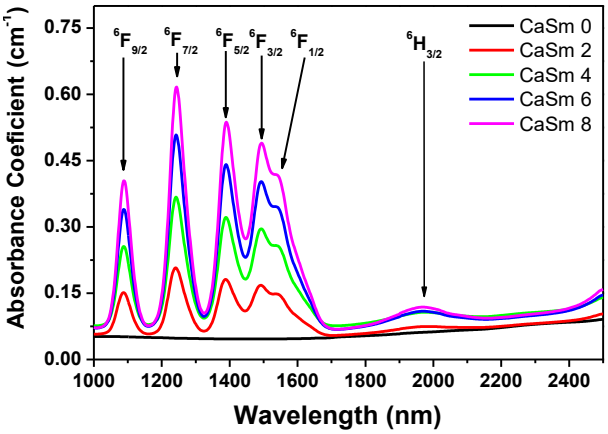


**Fig. 4:** (a) Optical absorption and electronic spectra and absorption coefficient of prepared glasses in the range from 300 to 500 *nm* and (b) NIR absorbance spectral date with the range from 1000 to 2400 *nm*

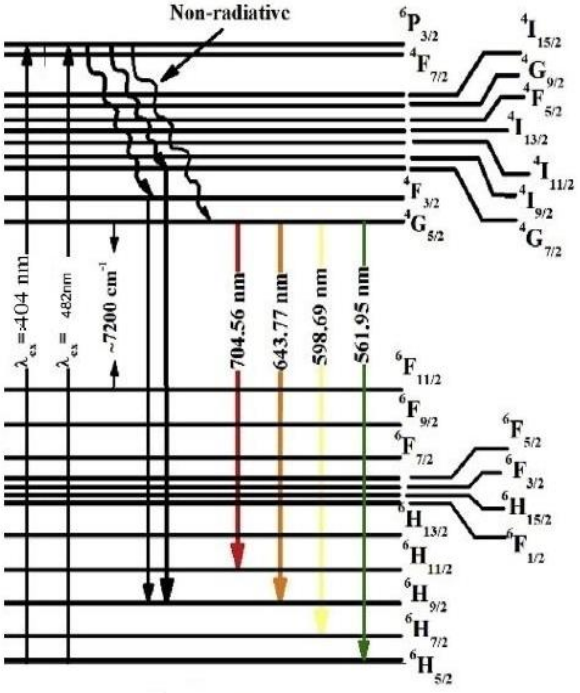


**Fig. 5:** Schematic representation of the $Sm^{3+}$ energy level diagram (up arrows) and emission routes (down arrows) are indicated (Lin et al., 2005) [52].

*3.4.2 Optical band gap energy*

According to Fig. 6, raising the $Sm_2O_3$ concentration causes a reduction in the optical energy gap. Table 2 displays the direct band gap as a function of photon energy for each glass system. Using the relation [53], the absorption (A) is changed into the absorption coefficient ($\alpha$):

$$\alpha(v) = (1/d)\ \ln(I_o/I) \qquad (3)$$

where d is the sample thickness and $ln(I_o/I)$is the absorbance (A). Using the conventional relation suggested by Davis and Mott function, the absorption (A) can be converted into a value proportionate to the absorption: [54,55]

$$\alpha h\nu = B(h\nu - E_g)^n \qquad (4)$$

Tauc plots of $(\alpha h\nu)^n$ versus $h\nu$ (with $n$=1/2, applicable for a direct bandgap material), as shown in **Fig. 6** and the extracted band gap plotted as a function of $Sm_2O_3$ concentration. The direct band gap is found to decrease from 5.78eV for $x$ = 0.0 mol %to 5.51eV for $x$ = 8.0 mol %. Many factors may control the values of optical band gap for studied materials including the degree of structural ordering (crystallinity)-disordering (amorphoucity), the type of dopants (donor/ acceptor), and/or carrier concentration in addition to the creation of materials. The formation of a phosphate glass matrix, which contributes to bonding defects in the network matrix of the equipped glasses due to the inclusion of rare earth dopant, tailors the band structure of the glasses at UV-edge, is credited with this decrease in optical band gap.

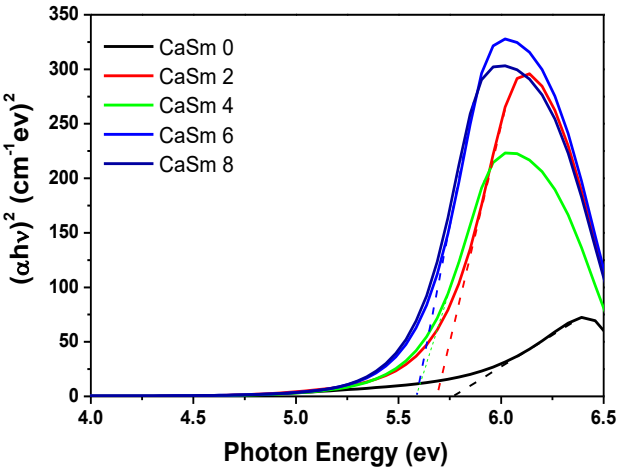


**Fig. 6:** The Optical band gap energy of $Sm^{3+}$ ion doped aluminum sodium phosphate glass ($x$ = 0, 2, 4, 6 and 8 mol%)

According to the Davis Mott approach, defects will produce localized states in the band gap [56]. As a result, the width of the localized states increases because of the increase in defect concentration and consequently reduces the Eg, this can be confirmed from the values of Urbac energy (table 2) which specify the width of tail states. Fig.7 shows the variations of Ln $\alpha$ versus h$\nu$ which obeys Urbac function:

$$\propto = \propto_0 e^{\frac{h\nu}{E_u}}$$

where $\alpha$o is a constant, h$\nu$ is the photon energy and $E_u$ is the Urbac energy. The slopes of the straight lines of these curves were used to determine the values of $E_U$. Obviously, the value of $E_U$ increases with the increase of Sm doping, indicating the presence of structure disorder due to the formation of certain defects and/or impurities that create localized states in the band structure

**Table 2:** Calculated optical energy gap in relation to $Sm_2O_3$ concentration

| Sample | Sm 0% | Sm 2% | Sm 4% | Sm 6% | Sm 8% |
|---|---|---|---|---|---|
| $E_g$ (eV) | 5.784 | 5.667 | 5.570 | 5.546 | 5.514 |
| $E_U$ eV) | 0.57803 | 0.58391 | 0.58229 | 0.58333 | 0.65333 |

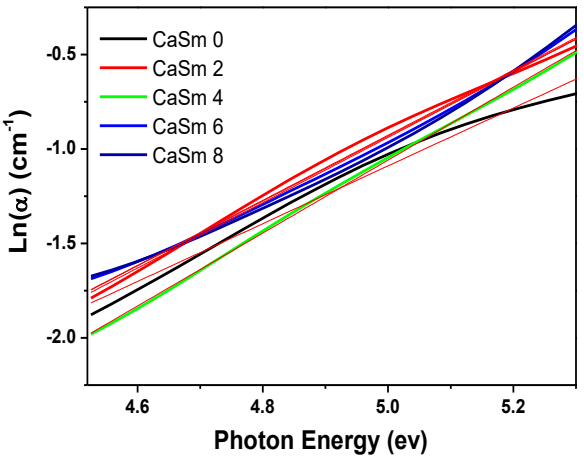


**Fig. 7:** The Urbac energy of $Sm^{3+}$ ion doped aluminum sodium phosphate glass ($x$ = 0, 2, 4, 6 and 8 mol%)

*3.4.3 Refractive index, Extinction coefficient, and complex dielectric constant*

The local field of the host material and the polarizability of ions are related to the refractive index. For every device design, including optical implementations like filters, the determination of the refractive index is crucial [57]. Equation [58] was used to determine the refractive index:

$$A + T + R = 1 \qquad (5)$$

where *A, E and T are* absorbances, transmittance, and reflectance respectively. The refractive index ($n$) therefore, can be calculated using equation (6) shown in **Fig. 8** [58]:

$$R = \frac{(n-1)^2}{(n+1)^2} \qquad (6)$$

It was concluded that there is an inverse relationship between refractive index and optical band gap and can be correlated with the density and molar volume of the synthesized materials [59, 60]. It was observed that density changes from 2.617 to 2.731 $g/cm^3$ to an energy gap that change from 5.784 *eV* to 5.514 *eV*. The conclusion reached was that the refractive index can be seen of as a compositional variable that is affected by a variety of other parameters, such as the optical basicity of glass, the polarizability of ions within the network structure, and the coordination number of ions [61].

Typically, the equation given in Fig. 9 is used to compute the extinction coefficient:

$$k = \frac{\alpha\lambda}{4\pi} \qquad (7)$$

where the absorption coefficient and wavelength, respectively, are represented by $\alpha$ and λ. It is seen that the extinction coefficient (k) increases with increasing $Sm^{3+}$ ion content within the aluminum sodium phosphate glass from 0.0 to 1.0 mol.%. The relationships illustrated in Fig. 10 are used to obtain the dielectric constants:

$$\varepsilon' = n^2 - k^2 \qquad (8)$$

$$\varepsilon'' = 2nk \qquad (9)$$

where $n$ is the refractive index, $k$ is the extinction coefficient, $\varepsilon'$ the real part and $\varepsilon''$ is the imaginary part.

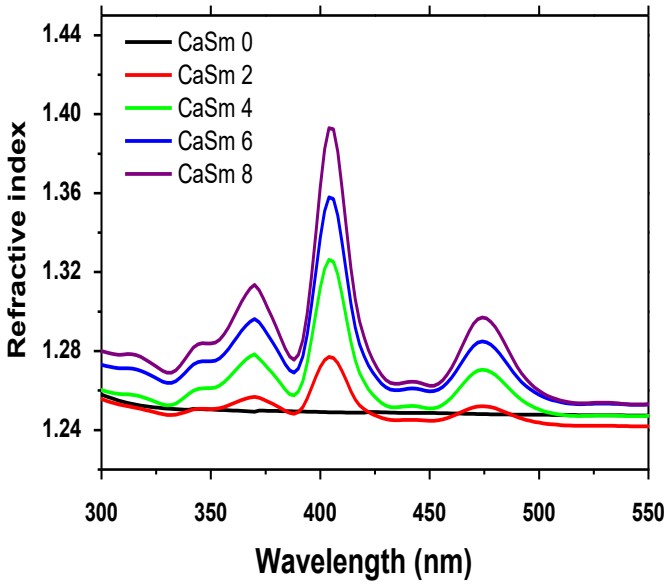


**Fig. 8:** Refractive index of $Sm^{3+}$ ion doped aluminum sodium phosphate glass ($x$ = 0, 2, 4, 6 and 8 mol%)

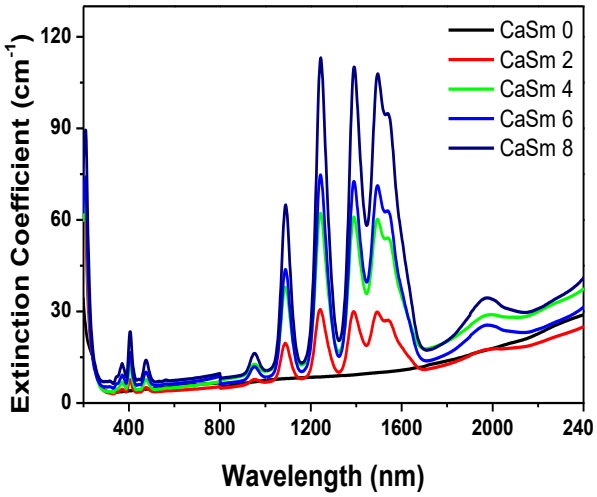


**Fig. 9:** Extinction coefficient of $Sm^{3+}$ ion doped aluminum sodium phosphate glass ($x$ = 0, 2, 4, 6 and 8 *mol%*).

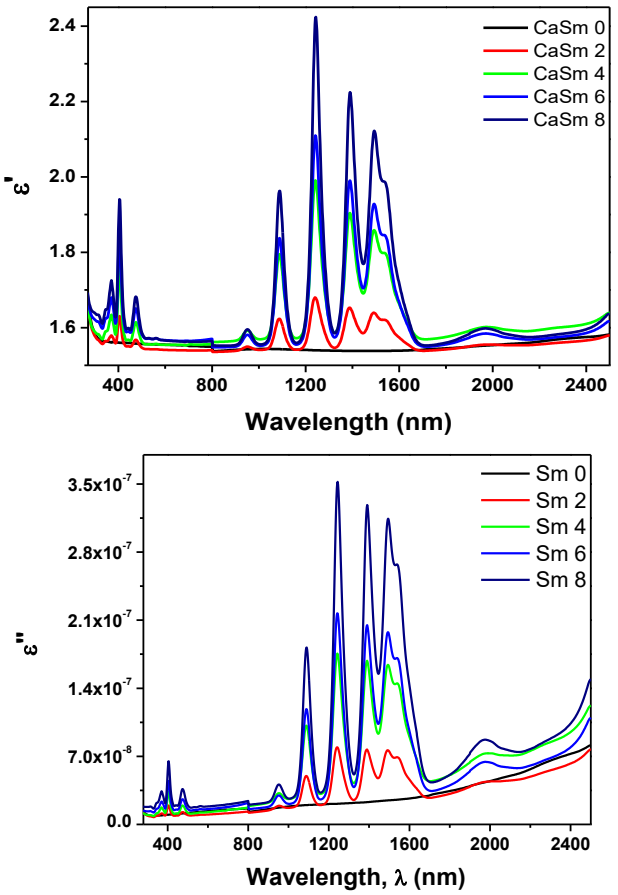


**Fig.10:** (a) The real permeability ($\varepsilon'$) and (b) the imagine permeability ($\varepsilon''$) vs. the wavelength of $Sm^{3+}$ ion doped aluminum sodium phosphate glass ($x$ = 0, 2, 4, 6 and 8 *mol%*)

## Conclusions

The current research demonstrates the impact of glass phosphate $Sm^{3+}$ ion, the molar volume, and density are researched to portray the phosphate glass $Al^{3+}$ ion impact and the uncommon increase in density and molar volume. As the samarium content increases, the density of the glass samples increases. Fourier transforms infrared FT-IR absorption spectra of all samples to maintain the phosphate glass matrix's primary characteristic absorption band and approves the existence of aluminum in both tetrahedral and octahedral conditions. Due to f-f transitions of $Sm^{3+}$ ions to distinct excited states, the optical absorption spectrum of the $Sm^{3+}$ ion-doped aluminium sodium phosphate glass matrix contains inhomogeneous bands of different intensities. The optical spectrum shows that these transitions' UV-visible area intensity is lower than their NIR region intensity. With increasing $Sm^{3+}$ ions concentration from 0.0 to 8.0 mol%, the direct band gap is observed to decrease from 5.78 eV to 5.51 eV. This is attributed to structural changes and the formation of phosphate glass matrix, which causes bonding defects in the network matrix of the prepared glasses because the addition of lanthanide dopant tailors the band structure of the glasses at UV-edge. The host glass and overlapping of different 2S+1LJ levels are used to explain the enhanced absorption as occurring in the UV-visible range. Research on the refractive index, extinction coefficient, and other optical properties reveals that there is little to no change with changing wavelength.

## References

[1] Borrero-Gonzalez LJ, Terra IAA, Nunes LAO, Farias AM, Barboza MJ, Rohling JH, Medina AN, Baesso ML, " The influence of $SiO_2$ content on spectroscopic properties and laser emission efficiency of $Yb^{3+}$-$Er^{3+}$ co-doped calcium aluminosilicate glasses", Appl. Phys. B, 2012, 107: 415

[2] Kotb IE, Okasha A, Marzouk SY, Zidan NA, "Extensive study on the optical and structural characteristics of Nd3+ doped Lead-Borate-Strontium-Tungsten glass system: Judd–Ofelt analysis", 2023, Results in Chemistry, 100869.

[3] Venkatramu V, Vijaya R, Leon-Luis SF, Babu P, Jaya-sankar C., Lavin V, Dhareshwar LJ, "Fluorescence and Spectroscopic Properties of $Yb^{3+}$-Doped Phosphate Glasses, J. Alloys Compd. ,2011, 509: 5084

[4] Zhang Q, Chen G, Zhang G, Qiu J, Chen D, "Infrared luminescence of Tm3+/Yb3+ codoped lanthanum aluminum germanate glasses", J. Appl. Phys., 2010, 107: 023102

[5] Pan Z, Morgan SH, Loper A, King V, Long BH,. Collins WE, "Infrared to visible upconversion in $Er^{3+}$-doped-lead-germanate glass: Effects of $Er^{3+}$ ion concentration" J. Appl. Phys.,1995, 77: 4688

[6] Lahoz F, Haro-Gonzalez P, Rivera-Lopez F, Gonza lez-Perez S, Martin IR, Capuj NE, Afonso CN, Gonzalo J, Fernandez J, Balda R, "Upconversion emission in Er3+-doped lead niobium germanate thin-film glasses produced by pulsed laser deposition" 2008, Appl. Phys. ,A 93: 621

[7] Kassab LRP, Bomfim FA, Martinelli JR, Wetter NU, Neto JJ, de Arau´jo CB, "Energy transfer and frequency upconversion in $Yb^{3+}$–$Er^{3+}$-doped PbO-$GeO_2$ glass containing silver nanoparticles" Appl. Phys., 2009, B 94: 239

[8] Fuchi S, Sakano A, Mizutani R, Takeda Y, Appl. Phys. B, 2011, 105: 877

[9] Barik SK, Senapati A, Balakrishnan S, Ananthasivan K, "Optimization of $Bi_2O_3$–$B_2O_3$-based glass phosphor co-doped with $Yb^{3+}$ and $Nd^{3+}$ for optical coherence tomography light source", Progress in Nuclear Energy, 2022, 152: 104372.

[10] Duan Z, Zhang J, Hu L, "Spectroscopic properties and Judd-Ofelt theory analysis of Dy3+ doped oxyfluoride silicate glass", J. Appl. Phys., 2007, 101: 043110

[11] Babu S, Jang K, Cho EJ, Lee H, Jayasankar CK, "Thermal, structural and optical properties of $Eu^{3+}$-

doped zinc-tellurite glasses", J. Phys. D Appl. Phys., 2007, 40: 5767
[12] Qiao X, Fan X, Wang M, Zhang X, "Spectroscopic properties of $Er^{3+}$ and $Yb^{3+}$ co-doped glass ceramics containing $SrF_2$ nanocrystals", J. Phys. D Appl. Phys., 2009, 42: 055103
[13] Jiang XP, Yang ZM, Liu T, Xu SH, "Energy transfer between Yb3+ and Er3+ in barium gallogermanate glass" J. Appl. Phys. ,2009, 105: 103113
[14] Ghigna P, Tomasi C, Speghini A, Bettinelli M, Scavini M, "Local chemical environment of Nd3+, Eu3+, and Er3+ luminescent centers in lead germanate glasses", J. Appl. Phys. 2009, 105: 023519
[15] Som T, Karmakar B, "Optical properties of Eu3+-doped antimony-oxide-based low phonon disordered matrices", J. Phys. Condens. Matter , 2010, 42: 035603
[16] Xu RR, Tian Y, Wang M, Hu LL, Zhang JJ, "Spectroscopic properties of 1.8 μm emission of thulium ions in germanate glas", 2011, Appl. Phys. B 102: 109
[17] Wei D, Yuan B, Huang Y, Tsuboi T, Seo HJ, "Influence of Crystallization on the Conversion of $Sm^{3+}\rightarrow Sm^{2+}$ in SrO–$Bi_2O_3$–$K_2O$–$B_2O_3$ Glass-Ceramics", J. Am. Ceram. Soc., 2013, 96: 2167
[18] Guan Y, Wei Z, Huang Y, Maalej R, Seo HJ, "1.55 μm emission and upconversion luminescence of Er3+-doped strontium borate glasses", Ceram. Int., 2013, 39: 7023
[19] Balda R, Fernandez J, Adam JL, Arriandiaga MA, "Time-resolved fluorescence-line narrowing and energy-transfer studies in a -doped fluorophosphate glass", Phys. Rev. B, 1996, 54:12076
[20] Van-Deun R, Binnemans K, Gorller-Walrand C, Adam JL, "Optical properties of-doped fluorophosphate glasses", J. Phys.: Condens. Matter, 1998, 10:7231
[21] Praveena R, Vijaya R, Jayasankar CK, " Photoluminescence and energy transfer studies of Dy3+-doped fluorophosphate glasses", Spectrochim. Acta, 2008, A70:577
[22] Babu S, Babu P, Jayasankar CK, Troster T, Sievers W, Wortmann G, " Optical properties of Dy3+-doped phosphate and fluorophosphate glasses" Opt. Mater., 2009, 31:624
[23] Basavapoornima C, Jayasankar CK, Chandrachoodan PP, "Luminescence and laser transition studies of Dy3+: K–Mg–Al fluorophosphate glasses", Physica B ,2009, 404:235
[24] Linganna K, Jayasankar CK, "Optical properties of Eu3+ ions in phosphate glasses", Spectrochim. Acta A, 2012, 97:788
[25] Sreedhar VB, Ramachari D, Jayasankar CK, "Optical properties of zincfluorophosphate glasses doped with Dy3+ ions", Physica B, 2013, 408:158
[26] Liao M, Hu L, Duan Z, Zhang L, Wen L, "Spectroscopic properties of fluorophosphate glass with high $Er^{3+}$ concentration", Appl. Phys. B, 2007, 86:83
[27] Tian Y, Zhang LY, Xu RR, Hu LL Zhang, JJ, "2 μm emission properties in $Tm^{3+}$/$Ho^{3+}$ codoped fluorophosphate glasses", Appl. Phys. B, 2010, 101:861
[28] Tian Y, Xu R, Zhang L, Hu L, Zhang J, "1.8 μm emission of highly thulium doped fluorophosphate glasses", J. Appl. Phys., 2010, 108:083504
[29] Brito TB, Vermelho MVD, Gouveia EA, de Araujo MT, Guedes I, Loong C-K, Boatner LA, "Optical characterization of Nd3+-and Er3+-doped lead-indium-phosphate glasses", J. Appl. Phys., 2007, 102:043113
[30] Santos EAF, Silva WF, de Arau´jo MT, Vermelho MVD, Guedes I, Loong C-K, Boatner LA, Jacinto C, Quantum efficiencies and thermo-optical properties of Er3+-, Nd3+-, and Pr3+-single doped lead-indium-phosphate glasses", J. Appl. Phys., 2009, 106:113111
[31] Santos CC, Rocha U, Guedes I, Vermelho MVD, Boatner LA, Jacinto C, "Thermal lens study of thermo-optical properties and concentration quenching of Er3+-doped lead pyrophosphate-based glasses", J. Appl. Phys., 2012, 111:123101
[32] Santos CC, Guedes I, Siqueira JP, Misoguti L, Zilio SC, Boatner LA, "Third-order nonlinearity of $Er^{3+}$-doped lead phosphate glass", Appl. Phys. B 99, 2010:559 [33] Churikov VM, Valeyev AI, Schavelev KO, Schavelev OS, "Large enhancement of second harmonic generation in highly cerium doped lead-phosphate glass", Opt. Mater. ,2002, 19:415
[34] Wahba EA, Alyousef HA, El-Rehim AA, Shaaban KS, "Large enhancement of second harmonic generation in highly cerium doped lead-phosphate glass", Journal of Electronic Materials, 2023, 52(1):219-236.
[35] Oo HM, Kamari HM, Wan-Yusoff WMD, " Optical properties of bismuth tellurite based glass", Int. J. Mol. Sci., 2012, 13:4623–4631.[36] Kaewjaeng S, Kaewkhao J, Limsuwan P, Maghanemi U, " Effect of BaO on optical, physical and radiation shielding properties of SiO2-B2O3-Al2O3-CaO-Na2O glasses system", Procedia Eng. 2012, 32:1080–1086.
[37] Limkitjaroenporn P, "Physical, optical, structural and gamma-ray shielding properties of lead sodium borate glasses", J. Phys. Chem. Solids 2011, 72:245–251.
[38] Dutta A, Ghosh A, " Structural and optical properties of lithium barium bismuthate glasses", J. Non-Cryst. Solids 2007, 353:1333–1336.
[39] Punia R, Kundu RS, Hooda J, Dhankhar S, Dahiya S, Kishore N, "Effect of Bi2O3 on structural, optical, and other physical properties of semiconducting zinc vanadate glasses", J. Appl. Phys., 2011:110
[40] Rashad MM, Mostafa AG, Mwakikunga BW, Rayan DA, "Tunable optical properties of some rare earth elements-doped mayenite $Ca_{12}Al_{14}O_{33}$ nanopowders elaborated by oxalate precursor route", Applied Physics A, 2017, 123:42, 1-7.
[41] Rashad MM, Mostafa AG, Rayan DA, "Structural and optical properties of nanocrystalline mayenite $Ca_{12}Al_{14}O_{33}$ powders synthesized using a novel route", J. Mater. Sci.: Mater. Electron., 2016, 27(3):2614-2623.
[42] Ewais EMM, Besisa DHA, El-Amir AAM, El-Sheikh SM, Rayan DE, "Optical properties of nanocrystalline magnesium aluminate spinel synthesized from industrial

wastes", Journal of Alloys and Compounds, 2015, 649:159-166.
[43] Liu T., Zhang Y, Shao H, Li X, " Synthesis and Characteristics of $Sm_2O_3$ and $Nd_2O_3$ Nanoparticles", Langmuir, 2003, 19 (18):7569–7572.
[44] Kang JG, Min B.K., Sohn Y, "Synthesis and characterization of $Sm(OH)_3$ and $Sm_2O_3$ nanoroll sticks", Journal of Materials Science, 2015, 50(4):1958–1964.
[45] Marzouk MA, ElBatal HA, Abdelghany AM, Ezz Eldin FM, "Ultraviolet, visible, ESR, and infrared spectroscopic studies of CeO2-doped lithium phosphate glasses and effect of gamma irradiation", Journal of Molecular Structure, 2011, 997(1-3):94-102.
[46] Marzouk MA, ElBatal FH, Abdelghany AM, "Ultraviolet and infrared absorption spectra of Cr2O3 doped–Sodium metaphosphate, lead metaphosphate and zinc metaphosphate glasses and effects of gamma", Spectrochimica Acta Part A: Molecular and Biomolecular Spectroscopy, 2013, 114:658-667.
[47] Okasha A, Abdelghany AM, Marzouk SY, "Judd–Ofelt analysis of spectroscopic properties of $Sm^{3+}$ doped $P_2O_5$–SrO glasses", Journal of Materials Science: Materials in Electronics, 2017, 28(16):12132–12138
[48] Seshadri M, Rao KV, Rao JL, Ratnakaram YC, "Spectroscopic and laser properties of Sm3+ doped different phosphate glasses", J. Alloys Compd. 2009, 476:263–270
[49] Judd BR, "Optical absorption intensities of rare-earth ions", Phys. Rev. 1962, 127:750–761
[50] Ofelt GS, "Intensities of crystal spectra of rare-earth ions", J. Chem. Phys., 1962, 37:511–520
[51] Khatab TK, Abdelghany AM, Shaker N, Osama Y, Kandil EM, "Evaluation of the Optical and Structural Properties of Constructed Bis-indole Derivatives Using ($Sm_2O_3$/$SiO_2$) Catalyst", Silicon, 2018, 10(5):2173–2179
[52] Lin H H, Yang D, Liu G, Ma T, Zhai B, An Q, Yu J, Wang X, Liu X, Pun E, "Optical absorption and photoluminescence in Sm3+-and Eu3+-doped rare-earth borate glasses", J. Luminescence, 2005, 113:121- 128.
[53] Abdel-Gayed MS, Elbashar YH, Barakat MH, Shehata MR, "Optical spectroscopic investigations on silver doped sodium phosphate glass", Optical and Quantum Electronics, 2017, 49 (9):305
[54] D. A. Rayan, A. M. Elseman, M. M. Rashad, "Remarkable impact of $Ni^{2+}$ ion on the structural, optical, and magnetic properties of hexagonal wurtzite ZnS nanopowders", Applied Physics A, 2018, 124: 659.
[55] Rashad MM, Ibrahim AA, Rayan DA, Sanad MMS, Helmy IM, "Photo-Fenton-like degradation of Rhodamine B dye from waste water using iron molybdate catalyst under visible light irradiation", Environmental Nanotechnology, Monitoring & Management, 2017, 8:175-186.
[56] Mott NF, Davis EA, Clarendon, 1979, p. 428. Oxford.
[57]. Yousef ES, "Linear and non-linear optical phenomena of glasses (photonics-photo chromic-electro and magneto optics): a review", Solid State Phenomena, 207, Trans Tech Publications ,2014:1-35
[58] Rayan DA, Elbashar YH, Rashad MM, El-Korashy A, "Optical spectroscopic analysis of cupric oxide doped barium phosphate glass for bandpass absorption filter", J. Non-Cryst. Solids, 2013, 382:52–56.
[59] Elkhoshkhany N, Samir Y. Marzouk, Mohamed A. Khattab, Shaimaa A. Dessouki, "Influence of Sm2O3 addition on Judd-Ofelt parameters, thermal and optical properties of the TeO2-Li2O-ZnO-Nb2O5 glass system", Materials Characterization, 2018, 144:274-286.
[60] Elkhoshkhany N, Marzouk SY, Shahin S, "Synthesis and optical properties of new fluoro-tellurite glass within (TeO2-ZnO-LiF-Nb2O5-NaF) system", J. Non-Cryst. Solids, 2017, 472:39-45
[61] Al-Qaisi B, "UV spectroscopy, refractive indices and elastic properties of the (76− x) TeO2· 9P2O5· 15ZnO· xLiNbO3 glass", Solid State Sci., 2013, 19:6-11.